CANADIAN THESES

THÈSES CANADIENNES

NOTICE

The quality of this microfiche is heavily dependent upon the quality of the original thesis submitted for microfilming. Every effort has been made to ensure the highest quality of reproduction possible.

If pages are missing, contact the university which granted the degree.

Some pages may have indistinct print especially if the original pages were typed with a poor typewriter ribbon or if the university sent us an inferior photocopy.

Previously copyrighted materials (journal articles, published tests, etc.) are not filmed.

Reproduction in full or in part of this film is governed by the Canadian Copyright Act, R.S.C. 1970, c. C-30. Please read the authorization forms which accompany this thesis.

AVIS

La qualité de cette microfiche dépend grandement de la qualité de la thèse soumise au microfilmage. Nous avons tout fait pour assurer une qualité supérieure de reproduction.

S'il manque des pages, veuillez communiquer avec l'université qui a conféré le grade.

La qualité d'impression de certaines pages peut laisser à désirer, surtout si les pages originales ont été dactylographiées à l'aide d'un ruban usé ou si l'université nous a fait parvenir une photocopie de qualité inférieure.

Les documents qui font déjà l'objet d'un droit d'auteur (articles de revue, examens publiés, etc.) ne sont pas microfilmés.

La reproduction, même partielle, de ce microfilm est soumise à la Loi canadienne sur le droit d'auteur, SRC 1970, c. C-30. Veuillez prendre connaissance des formules d'autorisation qui accompagnent cette thèse.

THIS DISSERTATION
HAS BEEN MICROFILMED
EXACTLY AS RECEIVED

LA THÈSE A ÉTÉ
MICROFILMÉE TELLE QUE
NOUS L'AVONS REÇUE

NL 339 (r 86/01)

Canada

National Library of Canada
Bibliothèque nationale du Canada

122 Ottawa, Canada
K1A 0N4

TC –

0-315-23319-2

CANADIAN THESES ON MICROFICHE SERVICE – SERVICE DES THÈSES CANADIENNES SUR MICROFICHE

PERMISION TO MICROFILM – AUTORISATION DE MICROFILMER

• Please print or type – Écrire en lettres moulées ou dactylographier

AUTHOR – AUTEUR

Full Name of Author – Nom complet de l'auteur

Date of Birth – Date de naissance

Canadian Citizen – Citoyen canadien

☒ Yes Oui ☐ No Non

Country of Birth – Lieu de naissance

Permanent Address – Résidence fixe

THESIS – THÈSE

Title of Thesis – Titre de la thèse

Degree for which thesis was presented
Grade pour lequel cette thèse fut présentée

Year this degree conferred
Année d'obtention de ce grade

University – Université

Name of Supervisor – Nom du directeur de thèse

AUTHORIZATION – AUTORISATION

Permission is hereby granted to the NATIONAL LIBRARY OF CANADA to **microfilm** this thesis and to **lend** or **sell copies of the film.**

The author reserves other publication rights, and neither the thesis nor extensive extracts from it may be printed or otherwise reproduced without the author's written permission.

L'autorisation est, par la présente, accordée à la BIBLIOTHÈQUE NATIONALE DU CANADA de **microfilmer** cette thèse et de **prêter** ou de **vendre des exemplaires du film.**

L'auteur se réserve les autres droits de publication; ni la thèse ni de longs extraits de celle-ci ne doivent être imprimés ou autrement reproduits sans l'autorisation écrite de l'auteur

ATTACH FORM TO THESIS – VEUILLEZ JOINDRE CE FORMULAIRE À LA THÈSE

Signature

Date

NL 91 (r 84/03)

Canada

THE UNIVERSITY OF ALBERTA

RADIO FREQUENCY ENERGY DEPOSITION IN SALINE PHANTOMS

by

© JOHN ANTHONY ANTOLAK

A THESIS

SUBMITTED TO THE FACULTY OF GRADUATE STUDIES AND RESEARCH

IN PARTIAL FULFILMENT OF THE REQUIREMENTS FOR THE DEGREE

OF MASTER OF SCIENCE

DEPARTMENT OF PHYSICS

EDMONTON, ALBERTA

FALL 1985

THE UNIVERSITY OF ALBERTA

RELEASE FORM

NAME OF AUTHOR JOHN ANTHONY ANTOLAK

TITLE OF THESIS RADIO FREQUENCY ENERGY DEPOSITION IN SALINE PHANTOMS

DEGREE FOR WHICH THESIS WAS PRESENTED MASTER OF SCIENCE

YEAR THIS DEGREE GRANTED FALL 1985

(SIGNED) .....

PERMANENT ADDRESS:

.....

.....

.....

DATED 19

THE UNIVERSITY OF ALBERTA

FACULTY OF GRADUATE STUDIES AND RESEARCH

The undersigned certify that they have read, and recommend to the Faculty of Graduate Studies and Research, for acceptance, a thesis entitled RADIO FREQUENCY ENERGY DEPOSITION IN SALINE PHANTOMS submitted by JOHN ANTHONY ANTOLAK in partial fulfilment of the requirements for the degree of MASTER OF SCIENCE.

.....
Supervisor

.....

.....

.....

Date.....

Abstract

In the past decade, nuclear magnetic resonance has been increasingly used as a medical tool for studying the human body. During this period, there has been a substantial increase in the typical magnetic field strengths and resonating frequencies used in such *in vivo* NMR studies, because of the better signal-to-noise ratio and spectral resolution provided. Electric fields associated with radio frequency pulses applied to the irradiating coil in the NMR apparatus cause rf currents to flow in the living tissue being studied. These currents give rise to Joule heating or energy deposition in the tissue. Since rf heating increases rapidly with increasing frequency for a given amplitude of rf magnetic field, NMR examinations of patients at high frequencies may cause hyperthermia in sensitive organs and fluids, e.g. the orbit and CSF. It is therefore essential to obtain a proper understanding of the rf heating phenomenon as it occurs in *in vivo* NMR.

In this thesis, we describe Q-meter measurements of the rf losses in a series of saline samples (or phantoms) as a function of frequency and electrical conductivity. Measurements made using solenoidal and saddle coils, approximately 2.5cm in diameter, were found to be in satisfactory agreement with the predictions of a lumped circuit model similar to those proposed by Gadian and Robinson, and Vermeulen and Chute. In particular, the three parameters obtained by fitting the data to the model were

used to predict the rf heating to be expected if the samples investigated were subjected to an rf pulse in an NMR experiment using the same coils. The method used to fit the data enables the heating caused by the induced electric field to be distinguished from that caused by secondary electric fields associated with charges on the coil. We have used our data to calculate the heating expected in coils and samples of larger, but geometrically similar, dimensions to ours, by the use of a scaling factor which is easily calculated. Our results suggest that the rf heating in *in vivo* NMR examinations may cause the tissue temperature to rise to dangerously high values, if carried out at frequencies aproaching 100MHz.

The validity of our scaling procedure was checked by comparing the rf losses in a series of saline solutions situated, firstly, in a 2.75cm diameter saddle coil, and secondly, in an 11cm diameter saddle coil. In the second case, the linear dimensions of the coil, coil former and samples were four times larger than in the first case. The data confirmed the validity of the scaling procedure, except for a systematic deviation in the data for the larger coils, which is attributed to skin depth effects ignored in the model.

Acknowledgements

I wish to express my sincere appreciation to Dr. D.G. Hughes and Dr. P.S. Allen for suggesting this project and for their patient guidance and help.

I would like to thank the technical staff of the Department of Physics. Without their help, much of this work would have been impossible. I would also like to thank Mr. D. Ellinger for measuring the conductivities of some of the samples.

I would like to express my gratitude to the Natural Sciences and Engineering Research Council for awarding me a Postgraduate Scholarship and for financial support of this project.

Table of Contents

Chapter — Page

I. Introduction 1

II. Theory 3

A. Basic Theory of NMR 3

B. Origin of electric fields in NMR coils and samples 7

C. Calculation of the power dissipated by induced currents in conducting samples of cylindrical geometry 8

i) Magnetic field parallel to the cylinder axis 8

ii) Magnetic field perpendicular to the cylinder axis 10

D. Analysis of the lumped circuit model of rf losses in conducting samples 11

E. Heating of samples caused by rf pulses 14

F. Size dependence of the heating caused by rf pulses 15

III. Experimental Details 17

A. Determination of Y_r 17

B. Coils used for the determination of Y_r 22

C. Description of the saline phantoms 24

D. Signal sources for the Q-meter 26

i) Low frequency measurements (<50MHz) 26

ii) High frequency measurements (30-100MHz) 26

E. Experimental procedure 27

IV. Results and Discussion 31

A. Analysis of the Y_r data 31

B. Calculation of the heating caused by rf pulses 37

C. Size dependence of the heating caused by rf pulses 42

D. Comparison of the heating produced by two variants of a commonly used imaging technique ..44

V. Conclusion 46

References 47

List of Tables

Table Page

1. Values of the fitted parameters. 36

List of Figures

Figure — Page

1. Schematic diagram of the secondary electric field of a solenoidal coil. 9

2. Lumped circuit model of rf losses in conducting samples. 12

3. Series and shunt representations of a lossy inductor. 18

4. Schematic diagram of the measuring circuit of the Q-meter. 20

5. Saddle coil configuration. 23

6. Block diagram of the high frequency measuring circuit of the Q-meter. 28

7. Plots of Y_r/σ versus f/σ for the six-turn solenoid, the 2.3cm diameter series saddle coil and the 2.2cm diameter parallel saddle coil. 33

8. Plots of Y_r/σ versus f/σ for the 2.75cm and 11cm diameter series saddle coils. 34

9. Plots of Y_r/σ versus f/σ for the 2.75cm and 11cm diameter parallel saddle coils. 35

10. Calculated frequency dependence of the temperature rise per pulse for the six turn solenoid, the 2.3cm diameter series saddle coil and the 2.2cm diameter parallel saddle coil. 38

11. Calculated frequency dependence of the temperature rise per pulse for the 2.75cm and 11cm diameter series saddle coils. 39

12. Calculated frequency dependence of the temperature rise per pulse for the 2.75cm and 11cm diameter parallel saddle coils. 40

Chapter I

Introduction

For almost four decades, nuclear magnetic resonance (or NMR) has been an invaluable tool for chemists and physicists studying molecular structure and dynamical processes. However, it is only in the past decade that its usefulness as a non invasive method of medically studying the human body has been realized. In *in vivo* NMR studies, as in chemistry and physics, there has been a tendency to use stronger magnetic fields and higher resonating frequencies because they provide better signal-to-noise ratios and improved spectral resolution. This allows for shorter experimental times and hence less inconvenience for patients.

Electric fields associated with the irradiating coil or coils in the NMR apparatus will cause high frequency electric currents to flow in conducting samples. Although biological tissue is not very conductive compared to metals for example, the Joule heating associated with currents in the tissues can pose a danger to the living cells if the temperature rise exceeds about one degree Celsius (Schwan, 1982; Coupland et al., 1983). It is widely known that radio frequency heating of conducting material is a rapidly increasing function of frequency (Gandhi, 1975; Gadian and Robinson, 1979; Chute, Vermeulen, and Cervenan, 1981; Vermeulen and Chute, 1983). Therefore, because of the trend toward the use of higher frequencies in *in vivo* NMR,

experiments must be done to ensure that the amount of temperature rise (hyperthermia) will not be dangerous to the subject.

This thesis describes an experimental study of the conductivity, frequency and size dependence of radio frequency energy deposition in saline phantoms. The data are analyzed using a simple model of rf losses based on those proposed by Gadian and Robinson (1979) and Vermeulen and Chute (1983). The results are then used to predict the heat generated by rf pulses in the samples used. Furthermore, scaling is used to predict the heating that would occur in samples and coils more typical of those used in *in vivo* NMR.

Chapter II

Theory

A. Basic Theory of NMR

In the presence of a static magnetic field B_0, a nucleus of spin quantum number I and magnetic moment μ may occupy any of 2I+1 equally spaced energy levels given by

$$E_m = -m\mu B_0/I = -m\gamma\hbar B_0 \quad . \qquad (1)$$

In the above equation m is the z component of the spin quantum number which may take any value from -I to +I in integral steps, and γ, the magnetogyric or gyromagnetic ratio, is the ratio of the magnetic moment to the angular momentum of the nucleus. For a system of spins in thermal equilibrium, the population of each level is governed by the Boltzmann distribution which implies that the lower energy states are more heavily populated. This gives rise to a net magnetization $\underline{M}$ in the magnetic field direction. By applying a weak alternating magnetic field of frequency $f=\gamma B_0/2\pi$ perpendicular to the static field, magnetic dipole transitions, for which $\Delta m=\pm 1$, will be induced. Because of the excess population in the lower energy levels, energy will be absorbed by the spin system. In this way, information about the nuclear system may be extracted by monitoring the energy absorption. This is the method used in continuous wave (cw) NMR.

An alternative description of the NMR phenomenon can be given along the lines presented by Slichter (1978), and is particularly useful for discussing pulsed NMR. The equation of motion of a nucleus of magnetic moment μ subjected to a magnetic field $\underline{B}$ is given by

$$d_t \underline{J} = \underline{\mu} \times \underline{B} \qquad (2)$$

where d_t implies differentiation with respect to time and $\underline{J}$ is the angular momentum. Since $\underline{\mu}=\gamma\underline{J}$, this equation can be written as

$$d_t \underline{\mu} = \underline{\mu} \times (\gamma \underline{B}) \qquad (3)$$

This equation of motion is valid for any magnetic field, and implies that changes in $\underline{\mu}$ are perpendicular to both $\underline{\mu}$ and $\underline{B}$. In particular, a nucleus with its magnetic moment inclined at an angle to a constant magnetic field of magnitude B_o will precess about the $\underline{B}_o$ axis describing a cone.

Although equation (3) can be solved for arbitrary magnetic fields, it is instructive to view the motion of the magnetic moment of the nucleus from a rotating frame of reference. Notice in equation (3) that the cross product implies a rotation of $\underline{\mu}$ about $\underline{B}$ in a left hand sense if γ is positive. It is well known that

$$d_t\underline{\alpha} = \underline{\Omega} \times \underline{\alpha} \qquad (4)$$

describes the rotation of a vector $\underline{\alpha}$ about $\underline{\Omega}$ in a right hand sense with angular frequency equal to $|\underline{\Omega}|=\Omega$. Using equations (3) and (4), it can be shown that

$$\delta_t\underline{\mu} = \underline{\mu} \times (\gamma\underline{B}+\underline{\Omega}) \qquad (5)$$

where $\delta_t\underline{\mu}$ is the time rate of change of the magnetic moment in a frame rotating at an angular frequency Ω about $\underline{\Omega}$. If the magnetic field is equal to $\underline{B}_0$ and $\gamma\underline{B}_0+\underline{\Omega}$ vanishes, then the time derivative of the magnetic moment will be zero in the rotating frame. That is, $\underline{\mu}$ remains fixed with respect to the frame rotating about $\underline{B}_0$ at an angular frequency of γB_0.

Consider now the situation where, in addition to a static field $\underline{B}_0$ along the z axis, the nucleus is subjected to a sinusoidal alternating field of amplitude $2B_1$ and angular frequency ω directed along the x axis in the laboratory frame. It can easily be seen that

$$B_x = 2B_1\cos(\omega t) = B_1\{\exp(i\omega t) + \exp(-i\omega t)\} \qquad (6)$$

where $B_1\exp(i\omega t)$ and $B_1\exp(-i\omega t)$ are counter-rotating circularly polarized components of that field. If ω equals Ω, the angular frequency of rotation of the rotating frame, and $\underline{\Omega}=-\gamma\underline{B}_0$, then one of the rotating components will be a

static vector $\underline{B}_1$ along the x' axis where the prime denotes the rotating frame. The other component will have an angular frequency of 2ω in the rotating frame, and its effect on the nucleus may be ignored. Since $\underline{\Omega}=-\gamma\underline{B}_0$, the equation of motion for $\underline{\mu}$ in the rotating frame will therefore be

$$\delta_r\underline{\mu} = \underline{\mu} \times (\gamma\underline{B}_1) \qquad (7)$$

and it follows that $\underline{\mu}$ will precess about the x' axis with an angular frequency of $-\gamma B_1$. If the alternating field is turned on for a time τ then the magnetic moment will precess about $\underline{B}_1$ (or the x' axis) through an angle $\Theta=\gamma B_1\tau$, also referred to as the tip angle. In pulsed NMR, a pulse of length τ is referred to as a $\pi/2$ or 90° pulse if Θ is equal to $\pi/2$, and a π or 180° pulse if Θ is equal to π.

After a $\pi/2$ pulse, the magnetic moment lies in the x'-y' plane and, when viewed from the laboratory frame of reference, the magnetic moment is rotating about the z axis with an angular frequency of γB_0. The alternating magnetic field produced by the rotating magnetic moment can be detected by the voltage induced in a coil with its axis perpendicular to the z axis. Since there are no non-linear terms in the above equations, the equations presented here are equally valid for the net magnetization $\underline{M}$ of an assembly of identical nuclear magnetic moments. In this case, the equilibrium magnetization in a static field $\underline{B}_0$ is along the

$\underline{B}_0$ or z axis and a $\pi/2$ pulse applied along the x' axis will rotate $\underline{M}$ down to the -y' axis.

Note that the frequency of the field required for resonance is $f=\omega/2\pi=\gamma B_0/2\pi$. This is the same result obtained earlier from energy considerations.

B. Origin of electric fields in NMR coils and samples

It should be clear by now that an alternating magnetic field is required to perform NMR. Usually, this field lies in the radio frequency region of the electromagnetic spectrum.

Maxwell's equation,

$$\text{curl } \underline{E} = -\partial_t \underline{B} \qquad (8)$$

implies that a non-zero alternating electric field will be induced anywhere that the alternating magnetic field exists. This electric field gives rise to so-called induced currents in a conducting sample placed within the coil. In samples with cylindrical symmetry about the rf magnetic field direction, the current paths form concentric circles, hence the name eddy currents. In general, the currents are not necessarily at right angles to the magnetic field direction, but tend to be mainly perpendicular in many cases.

The other type of electric field generated by a coil is the secondary electric field produced by the charges associated with the voltage which exists on the coil. When

a conducting sample is placed in the coil, this electric field causes currents to flow. As can be seen in figure 1, the electric field and asociated currents are primarily axial near the centre of the coil. These currents have been referred to as dielectric currents by Gadian and Robinson (1979). However, we do not favour this because the term dielectric is usually reserved for non-conducting materials.

C. Calculation of the power dissipated by induced currents in conducting samples of cylindrical geometry

The power dissipated by induced currents for samples of arbitrary shape cannot be easily calculated. However, the power dissipated in cylindrical samples is amenable to theoretical treatment.

i) Magnetic field parallel to the cylinder axis

Consider a conducting cylinder of conductivity σ, radius ρ and length ℓ subjected to a uniform sinusoidal magnetic field $2B_1\cos(2\pi ft)$ applied along the x axis of the laboratory coordinate system. If the cylinder axis is also along the x direction then, by symmetry, the induced electric field will depend only upon the distance r from the axis of the cylinder. Using equation (8), it is easy to show that the amplitude of the electric field is given by

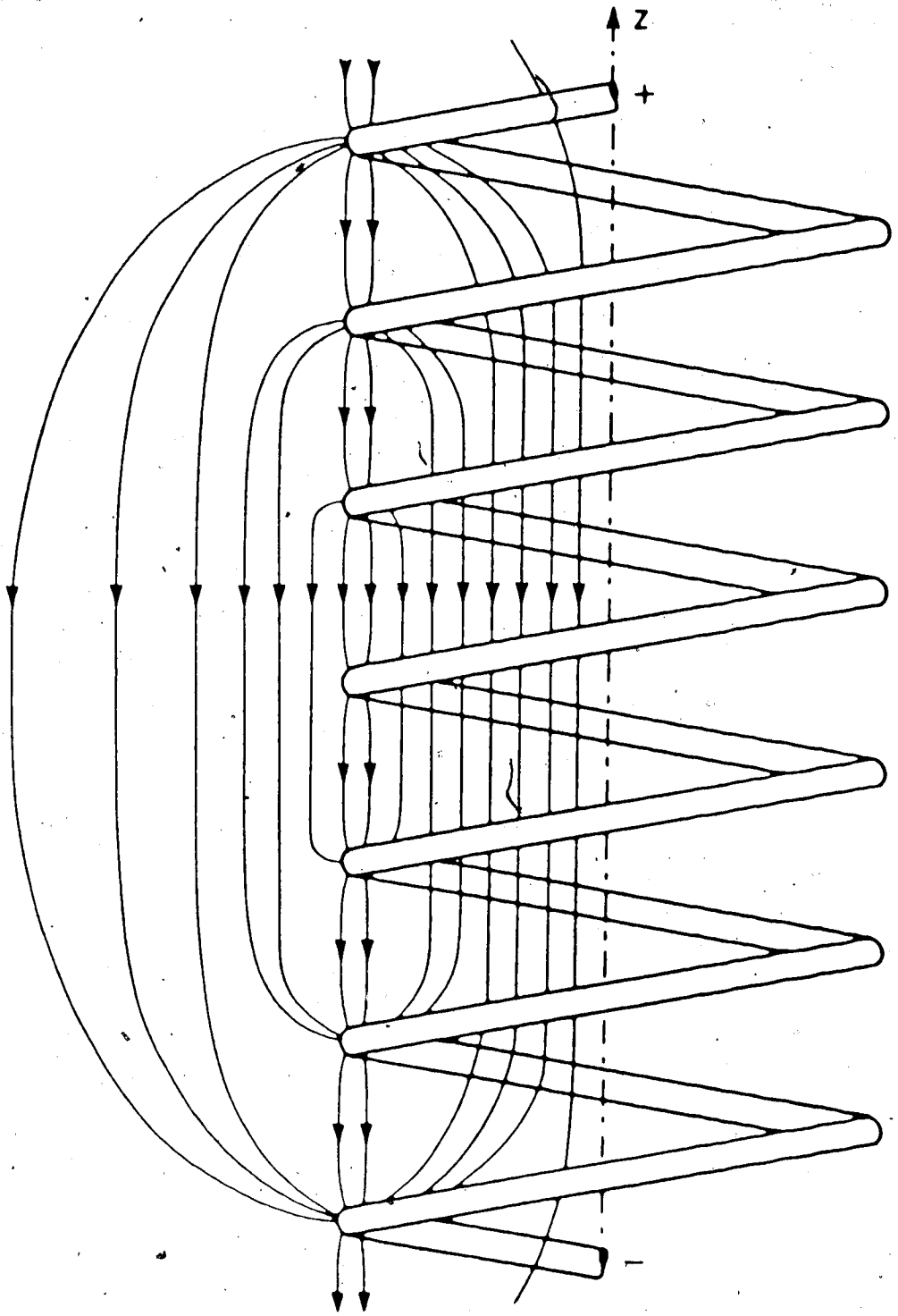

Figure 1. Schematic diagram of the secondary electric field of a solenoidal coil (Chute and Vermeulen, 1981).

$$E = 2\pi r f B_1 \ . \qquad (9)$$

The time average power dissipation per unit volume is $\sigma E^2/2$ and increases as the square of the distance from the centre of the cylinder. Integrating over the volume of the cylinder, the total power dissipation is given by

$$P = \sigma \pi^2 f^2 B_1^2 \rho^2 V \qquad (10)$$

where $V=\pi\rho^2\ell$ is the volume of the cylinder. Notice that, for a given volume, the total power dissipation increases as the square of the radius of the cylinder.

ii) **Magnetic field perpendicular to the cylinder axis**

If the cylinder is now oriented along the z axis, perpendicular to the uniform alternating magnetic field B_x, most of the symmetry disappears and the problem becomes very difficult to solve. However, if the cylinder length is extended to infinity, then translational invariance along the cylinder axis implies that all components of the induced electric field perpendicular to the cylinder axis must vanish. Using cartesian co-ordinates to solve equation (8), it is easy to see that

$$E_z = 4\pi y f B_1 \qquad (11)$$

and that the power dissipation per unit volume is proportional to the square of the distance from the x-z plane. Integrating over a section of the cylinder of length ℓ, the total power dissipation is

$$P = 2\sigma\pi^2 f^2 B_1^2 \rho^2 V \qquad (12)$$

where V is the volume of the cylinder section. Notice that this result is exactly twice the total power dissipation for the case where the cylinder axis is parallel to the field (cf. Bottomley, 1985).

D. Analysis of the lumped circuit model of rf losses in conducting samples

The model is based on those proposed by Gadian and Robinson (1979) and Vermeulen and Chute (1983) and is shown in figure 2. The empty coil is represented by L, C_o, and R. R_e represents the eddy current losses, C_1 represents the distributed capacitance between the coil and the sample, and R_d and C_2 represent the lossy sample. The admittance of the sample only is (cf. Gadian and Robinson, 1979)

$$Y_r = \frac{4\pi^2 f^2 R_d C_1^2}{1+4\pi^2 f^2 R_d^2 (C_1+C_2)^2} + R_e' \qquad (13)$$

$$Y_i = \frac{2\pi f C_1 + 8\pi^3 f^3 R_d^2 C_1 C_2 (C_1+C_2)}{1+4\pi^2 f^2 R_d^2 (C_1+C_2)^2} \qquad (14)$$

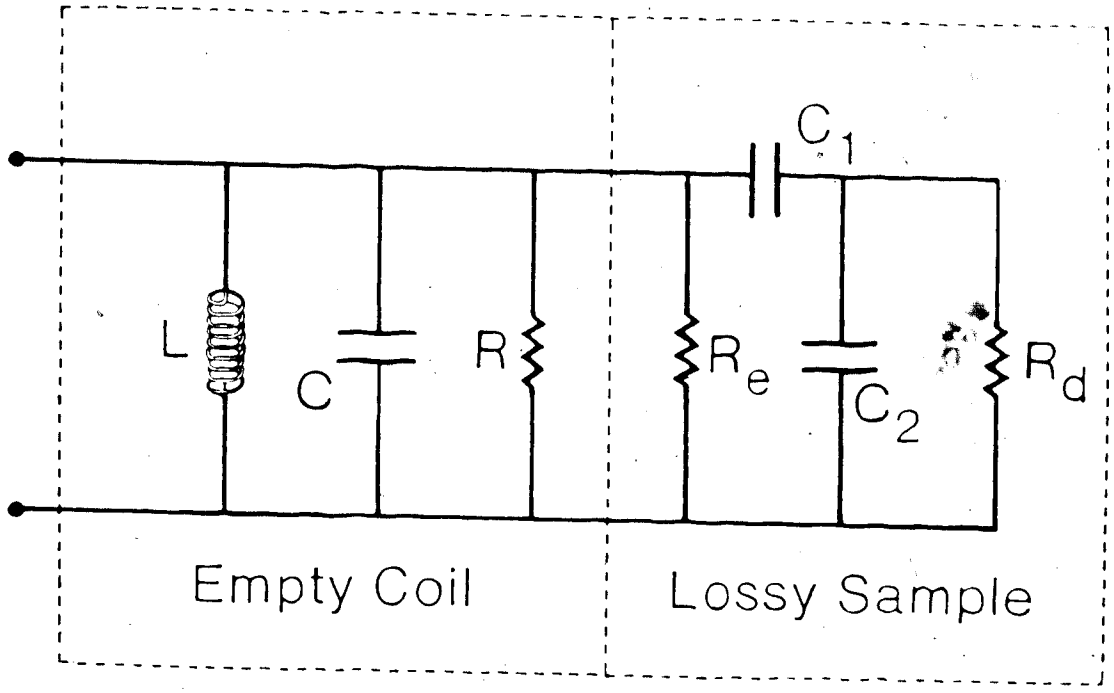

Figure 2. Lumped circuit model of rf losses in conducting samples.

where Y_r and Y_i are the real and imaginary parts of the admittance (Gadian and Robinson erroneously have a negative sign in the numerator of Y_i). Vermeulen and Chute (1983) have given expressions for R_e, R_d, C_1 and C_2 for a long solenoid. However, these expressions are not expected to be applicable to the types of coils used in *in vivo* NMR.

If R_e and R_d are assumed to be inversely proportional to the conductivity σ and independent of frequency, and C_1 and C_2 are constants, then the expression for Y_r can be rewritten as

$$Y_r = \sigma\{[A_1(\sigma/f)^2+A_2]^{-1} + A_3^{-1}\}, \qquad (15)$$

where

$$A_1 = (4\pi\sigma R_d C_1^2)^{-1} \qquad (16)$$

$$A_2 = \sigma R_d(1 + C_2/C_1)^2 \qquad (17)$$

$$A_3 = \sigma R_e \qquad (18)$$

are constants independent of frequency and conductivity. From equation (13), it appears that Y_r is governed by four independent parameters R_e, R_d, C_1 and C_2. However, we see from equation (15) that it is governed by only three parameters. This result does not appear in the literature, but is very useful in analyzing experimental values of Y_r as will be shown later.

E. Heating of samples caused by rf pulses

It is clear that the time average power dissipation in a sample is

$$P = V_0^2 Y_r / 2 \qquad (19)$$

where V_0 is the amplitude of the sinusoidal voltage applied to the coil. Since V_0 is equal to $2\pi f L I_0$ where I_0 is the amplitude of the current through the coil, then the power dissipation is given by

$$P = 2\pi^2 f^2 L^2 I_0^2 Y_r \qquad (20)$$

If the heat lost by the sample to the surroundings is ignored, the temperature rise during a rectangular rf pulse of length τ is

$$\Delta T \text{ per pulse} = 2\pi^2 f^2 L^2 I_0^2 Y_r \tau / W \qquad (21)$$

where W is the thermal capacity of the sample. Neglecting skin depth effects, the space average amplitude of the oscillating magnetic field $2B_1$ at the sample is bI_0 where b is a geometric factor independent of frequency. However, as was shown in §II.A, the tip angle of the nuclear magnetization is given by $\Theta = \gamma B_1 \tau$ so that

$$\Delta T \text{ per pulse} = 8\pi^2 f^2 L^2 \theta^2 Y_r / Wb^2 \gamma^2 \tau \ . \qquad (22)$$

Notice that the temperature rise per pulse is inversely proportional to the duration of the pulse for a given tip angle, an important result that does not, to our knowledge, appear in the literature.

F. Size dependence of the heating caused by rf pulses

Because of the difficulty of measuring rf losses in large coils and samples found in typical *in vivo* NMR systems, it is useful to consider the relationship between rf losses in coils and samples of similar geometry but different size. For a given NMR experiment (fixed f, θ, τ), the only parameters in equation (22) that are size dependent are W, b, L and Y_r. If the linear dimensions of a coil and sample are scaled by a factor λ, then W is obviously proportional to λ^3. The inductance of a coil of given geometry scales as λ as can be shown from the general (Neumann) formula for self inductance (Reitz, Milford, and Christy, 1979). Similarly, it can be shown from the Biot-Savart Law (Reitz, Milford, and Christy, 1979) that b is inversely proportional to λ, provided skin depth effects in the sample are neglected. Finally, since R_θ and R_d are inversely proportional to λ, while C_1 and C_2 are proportional to λ, it follows from equation (13) that Y_r is proportional to λ. Thus it can be seen from equation (22) that ΔT per pulse should be proportional to λ^2. Moreover,

it can be shown that the ratio of the power dissipation in the sample to the power dissipation in the coil is proportional to λ^2, assuming the skin depth of the wire is much smaller than the wire diameter.

Chapter III

Experimental Details

A. Determination of Y_r

Values of Y_r for various samples were found by measuring the Q-factor of the coil empty and when it contained the sample. The Q-factor of a high Q inductor is usually written as $2\pi fL/r$ where r is the series resistance as shown in figure 3(a). However, the model used to describe rf losses requires a consideration of parallel or shunt resistances. Figure 3(b) shows the shunt representation of a lossy inductor.

The relationship between r and R can be found by comparing the admittances of the series and shunt representations, which are

$$Y_a = \frac{r - i2\pi fL}{r^2 + 4\pi^2 f^2 L^2} \tag{23}$$

$$Y_b = \frac{2\pi fL - iR}{2\pi fLR} \tag{24}$$

where the subscripts a and b correspond to figure 3. Equating the real parts of the above equations gives

$$\frac{1}{R} = \frac{r}{r^2 + 4\pi^2 f^2 L^2} . \tag{25}$$

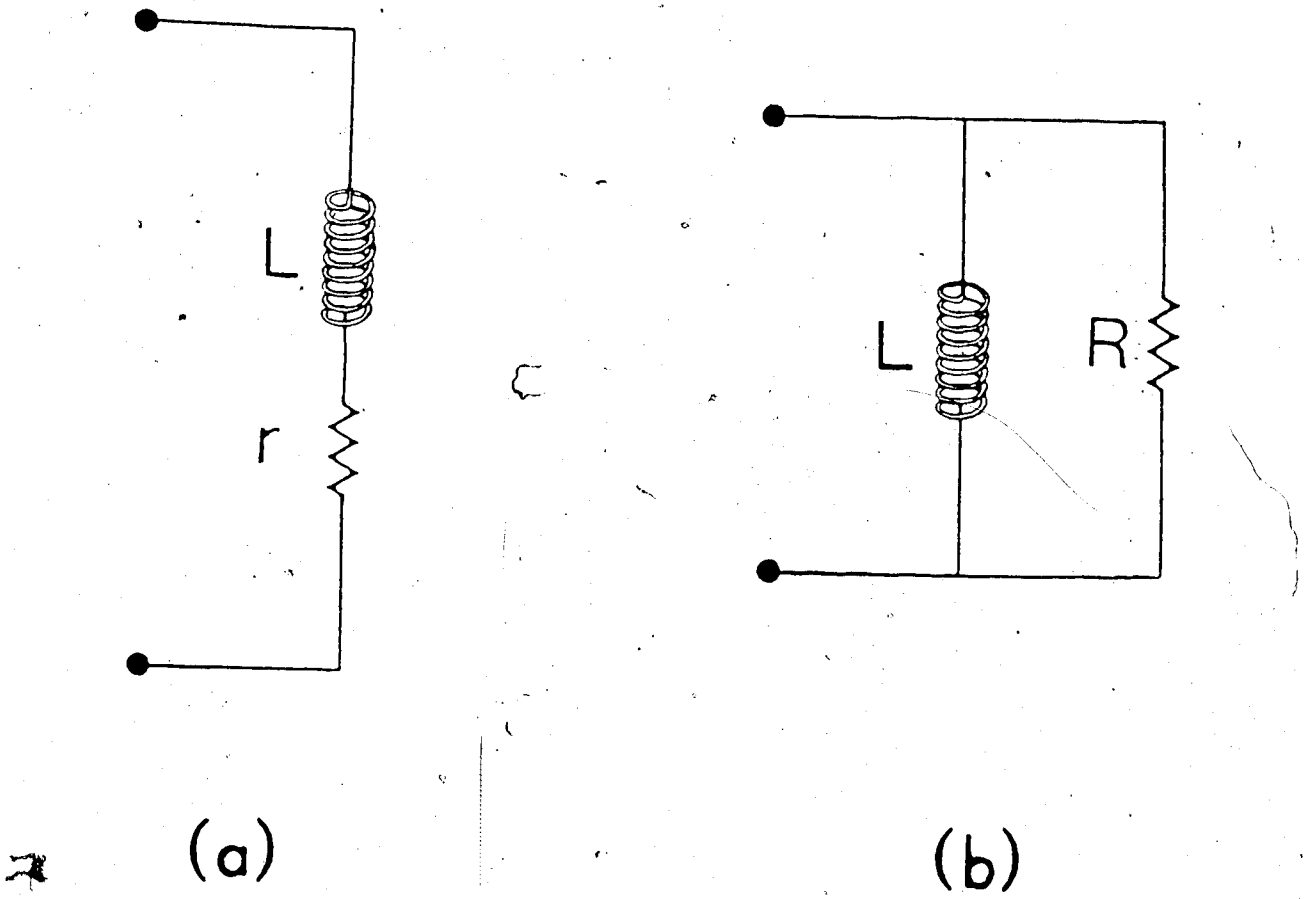

Figure 3. Series (a) and shunt(b) representations of a lossy inductor.

If Q is much greater than unity (which is true for our measurements), then $r^2+4\pi^2f^2L^2\cong4\pi^2f^2L^2$ so that $r=4\pi^2f^2L^2/R$. Substituting for r in the relation $Q=2\pi fL/r$ gives the result that $Q=R/2\pi fL$.

When the sample is placed in the coil, the total admittance is

$$R^{-1} + Y_r = (2\pi fLQ_s)^{-1} \qquad (26)$$

where Q_s is the Q-factor of the coil plus sample. The inductance is calculated using the resonance condition that

$$2\pi fC = (2\pi fL)^{-1} \qquad (27)$$

where C is the tuning capacitance used to resonate the coil. The final result is

$$Y_r = 2\pi f\{(C_s/Q_s)-(C/Q)\} \qquad (28)$$

where C_s is equal to C plus the capacitance due to the sample i.e. $Y_s/2\pi f$.

The Q measurements were made using a Marconi TF1245 Q-meter. A simplified schematic of this instrument is shown in figure 4, where L and r represent the coil and C is the instrument's resonating capacitance. As seen above, the Q of the coil is the ratio of the inductive reactance to the r[illegible]stance, or the ratio of the voltages across the

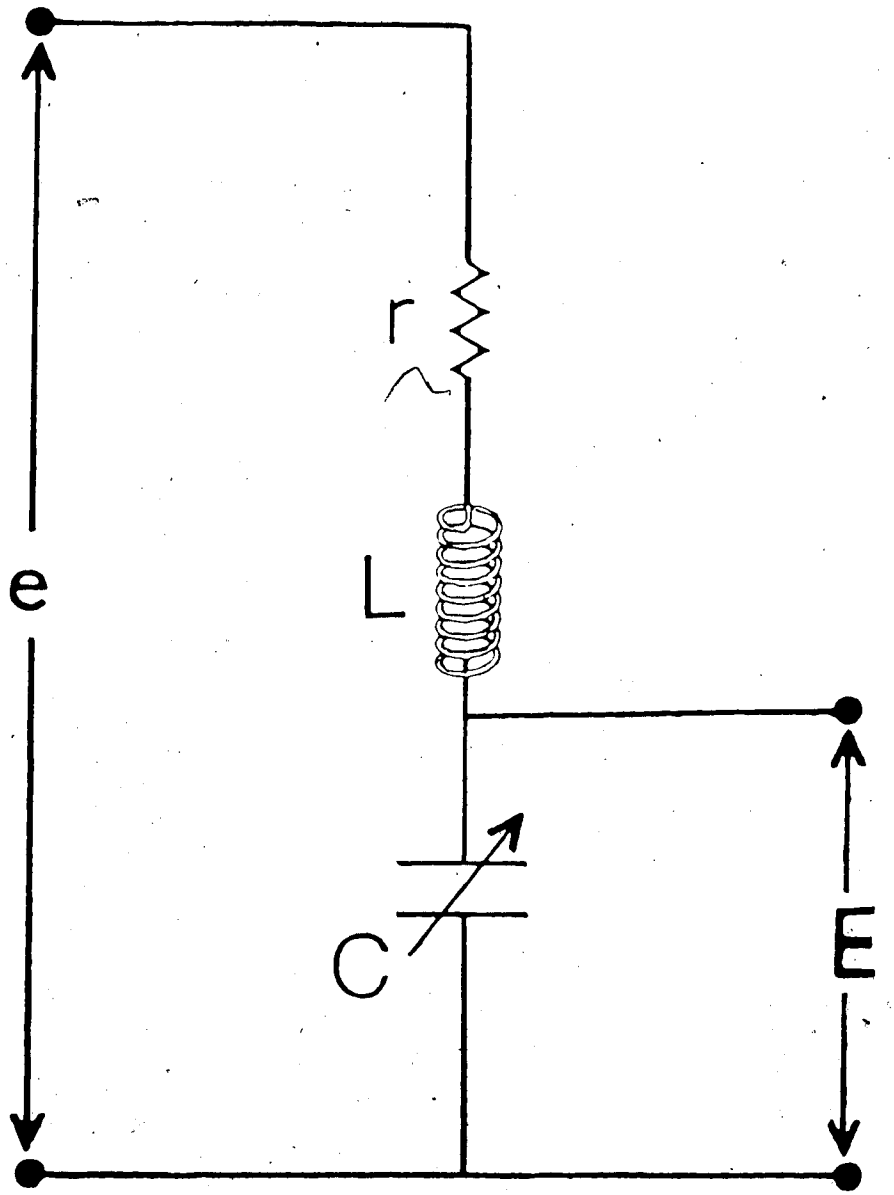

Figure 4. Schematic diagram of the measuring circuit of the Q-meter. L and r represent the external coil and C is the internal tuning capacitance. E and e are voltages measured by the instrument.

inductive and resistive components. Since the inductive reactance equals the capacitive reactance at resonance, the Q of the inductor is also equal to the ratio of the voltages generated across the capacitor and the resistor. At resonance, the voltages across L and C are equal but out of phase, which implies that e is equal to the voltage across r and that Q is equal to E/e.

In practice, the coil has a self capacitance C_o associated with it (which includes Y_i if the lossy sample is present). To obtain the true values of the Q and the resonating capacitance, the measured values of Q and C must both be multiplied by $(1+C_o/C)$. This implies that equation (28) remains valid even in the presence of C_o. The instrument itself has a residual inductance in series with the coil and the correction for this affects the indicated capacitance of the Q-meter, but not the indicated Q. This may be taken into account by rewriting Y_r as

$$Y_r = 2\pi f\{(C_1'/Q_1)-(C'/Q)\} \qquad (29)$$

where C' is the effective capacitance given by

$$C' = C/(1-4\pi^2 f^2 L_R C) \qquad (30)$$

and L_R is the residual inductance of the Q-meter and is given in the manual.

B. Coils used for the determination of Y_r

Measurements of Y_r were made on two different types of coils. The first coil was a six turn solenoidal coil made from #22 copper wire wound on a teflon former with an inside diameter of 1.9cm into which the samples were placed. The coil's diameter and length were 2.1cm and 1.6cm respectively.

A saddle coil configuration was used for the other coils because they are commonly used in *in vivo* NMR. Shown schematically in figure 5, a saddle coil creates a magnetic field perpendicular to the axis of the cylinder on which it is wound. The 60°-120° configuration is widely used in *in vivo* NMR since, in that case, the second derivatives of the magnetic field vanish at the centre of the coil (Ginsberg and Melchner, 1970), thereby ensuring a more homogeneous field.

The saddle coils used in the experiments were all single turn coils with only one wire on each of the current paths. However, two methods were used to connect the loops. For the "series" saddle coil, the current passes through one loop and then through the other loop. In the "parallel" saddle coil, half of the current goes through each loop. The inductance of the parallel saddle coil is smaller, which enables it to be tuned to higher frequencies, but its "field multiplier" b (see §II.E) is half that of the series saddle coil.

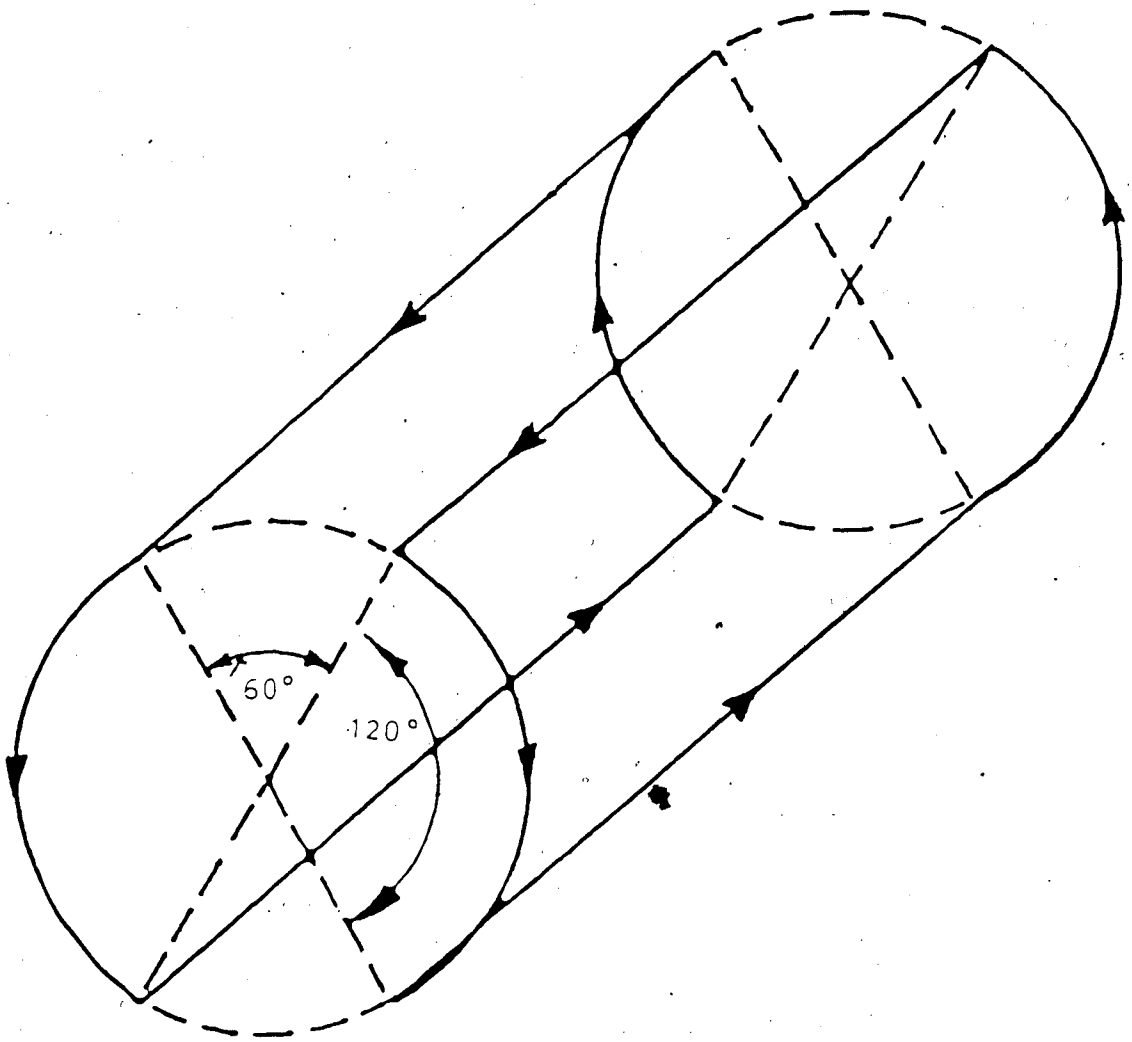

Figure 5. Saddle coil configuration. The arrows indicate the direction of current flow.

Parallel and series saddle coils were wound on to teflon formers very similar to that used for the six turn coil. The inside diameter of the formers was again 1.9cm and the coil diameters were between 2.2cm and 2.3cm. The length of the coils was 3.6cm giving a length to radius ratio of ≃3.2 which is quite close to 3.32, the value which gives the best field homogeneity (Mansfield and Morris, 1982).

To test the size dependence of rf losses, two more saddle coil formers were constructed from polyethylene, the larger one exactly four times the size of the smaller former. The inside diameter of the small former was 2.54cm and the coil diameter was 2.75cm. The wire size used for both parallel and series configurations was #20 for the small coils and #8 (four times the diameter) for the large coils. The length to radius ratio was 3.29 which is very close to the optimum value.

C. Description of the saline phantoms

The samples used with the teflon coil formers were contained in 3 dram glass vials with a volume of ≃11.2mℓ and an inside diameter of ≃1.6cm. Therefore, the gap between the sample and the coil varied between 1.5mm and 2.5mm depending upon the coil used. The sample extended approximately 2.4cm above the coil former when the sample was inserted. The saline solutions, prepared by Dr. L. Pandey who formerly worked in our laboratory, ranged

in concentration from 2mM to 3.5M.

For the large series saddle coil, 215.864g of reagent grade sodium chloride was dissolved to make 2ℓ of 1.847M solution. Approximately 250mℓ was set aside and 1.6ℓ was used to fill the large coil former. When the measurements were concluded, the solution was diluted 1:2 and the measurements were repeated. The solution was diluted nine times in total to give a final concentration of 3.607mM. The solutions set aside were used for the smaller 2.75cm diameter coils. A pipette was used to transfer 25mℓ of solution into the coil former. For measurements with the large parallel saddle coil, another 2ℓ solution of concentration 0.484M was made using 56.593g of sodium chloride. This solution was diluted a total of seven times to give a final concentration of 3.783mM.

The conductivities of the above solutions were calculated by interpolation of the data given by Robinson and Stokes(1959), and Chambers, Stokes, and Stokes(1956). With the help of Mr. D. Ellinger in the Department of Electrical Engineering, the conductivity of some of the solutions was measured using a vector impedance meter at 100Hz and found to be in good agreement with the calculated values.

D. Signal sources for the Q-meter

i) Low frequency measurements (<50MHz)

The values of Y_r for the 2.1cm to 2.3cm coils wound on teflon formers were obtained using a Marconi TF1246 oscillator as the signal source for the Q-meter. The TF1246 is designed with an output impedance of 0.5Ω to match the input impedance of the Q-meter. The frequency of operation is adjustable and an approximate value is indicated on a dial on the front panel of the instrument. However, for greater accuracy , it was decided to measure the the frequency independently using a frequency counter (Transistor Specialties, model 385R). Connecting the counter severely loaded the oscillator making Q measurements impossible. Using a spectrum analyzer, it was found that connecting the frequency counter also caused a shift in the ouput frequency, so that it was not possible to disconnect the counter to make measurements. To remedy this, a small capacitance was connected in series with the counter, so that accurate frequency measurements could be made. Some loading of the oscillator was still evident, but this was small enough so that measurements could be made with the counter connected.

ii) High frequency measurements (30-100MHz)

In order to test the validity of the lumped circuit model, we found it necessary to extend our measurements

towards 100MHz. However, the Marconi TF1247 oscillator recommended for use with the Q-meter from 20-300MHz was unavailable. A block diagram of the circuit used instead is shown in figure 6. The signal source was the rf output on the Hewlett-Packard 4815A vector impedance meter, and two potentiometers in the attenuator provided close control of the rf amplitude. The signal was boosted 50dB by a linear amplifier (Electronic Navigation Industries model 550L, maximum output 50 Watts) to satisfy the large power requirements of the TF1245 Q-meter. The Marconi TM5727 impedance matching unit was used to match the output impedance of the amplifier (50Ω) to the 0.5Ω input impedance of the Q-meter. The frequency was monitored by connecting the frequency counter directly to the HP 4815A vector impedance meter, which avoided loading the system.

E. Experimental procedure

Referring back to §III.B, the Q-factor of the coil is given by the ratio of the voltage on the capacitor to the voltage injected into the circuit. The TF1245 Q-meter measures the injected emf and displays the result as a Q multiplier. The voltage across the capacitor is displayed as a Q value. When the input voltage is adjusted so that the Q multiplier is unity, the Q-factor is read directly from the Q-meter. When the Q multiplier is not equal to one, the Q-factor is obtained by multiplication of the Q multiplier and the Q reading. According to the operating

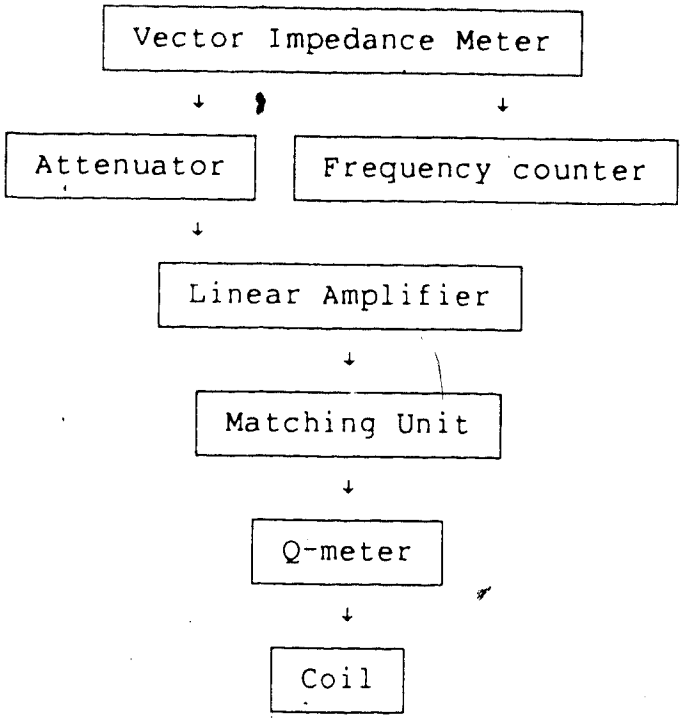

Figure 6. Block diagram of the high frequency measuring circuit of the Q-meter.

manual, the basic accuracy of the Q-meter reading is about 6% up to 100MHz. Some of the Q measurements were checked by measuring the bandwidth of the resonating circuit using both the Q-meter and the HP 4815A vector impedance meter. These values were found to be in agreement with the direct Q-meter readings.

The usual procedure for measuring Y_r was to first set the frequency and then adjust the zero of the Q-meter as described in the operating manual. The internal capacitor was adjusted for maximum deflection of the Q-meter needle and the values of the Q reading, Q multiplier and tuning capacitance were noted. The sample was placed in the coil, and the coil was retuned to give new values of the Q reading, Q multiplier and tuning capacitance. The sample was removed and the procedure repeated for another combination of sample conductivity and frequency. Using equation (29), the real part of the admittance was calculated for the various samples.

For the large 11cm diameter saddle coils this procedure could not be used because the stray field extended far beyond the coil. The presence of my hand near the coil to adjust the tuning capacitance detuned the coil so that finding resonance was almost impossible. In fact, the effect of placing my hand near the coil was comparable to the effect of inserting some of the samples in the coil. This effect was not observed with the smaller coils, because the extent of the stray field was proportionately smaller.

The above procedure was therefore modified so that the tuning capacitance was first set and then the frequency of the input adjusted for maximum deflection of the Q-meter needle. The sample was added and the coil was retuned by adjusting the input frequency. It is easy to show that the value of Y_r obtained from these measurements is given by

$$Y_r = 2\pi C'\{(f_s/Q_s)-(f/Q)\} \qquad (31)$$

where C' is the corrected tuning capacitance and f_s and f are the resonance frequencies with and without the sample.

Chapter IV

Results and Discussion

A. Analysis of the Y_r data

As shown in chapter II, the real part of the admittance is governed by the three parameters A_1, A_2 and A_3. Using the procedure described in chapter III, values of Y_r were obtained for various coil configurations, sample conductivities and resonating frequencies. By dividing both sides of equation (15) by the frequency, we find that

$$Y_r/f = (\sigma/f)\{[A_1(\sigma/f)^2+A_2]^{-1} + A_3^{-1}\} \qquad (32)$$

where the right hand side is now a function of the ratio of the conductivity and frequency. Similarly dividing both sides of equation (15) by σ gives

$$Y_r/\sigma = [A_1(\sigma/f)^2+A_2]^{-1} + A_3^{-1} \; . \qquad (33)$$

Values of Y_r/f were fitted to equation (32) using a non-linear least squares fitting FORTRAN subroutine (Bevington, 1969). Estimates of the standard error in Y_r/f were used as weighting factors in the fitting subroutine and were obtained by estimating the errors in the Q-factor and tuning capacitance. It was assumed that frequency errors were negligible.

Initial estimates of the three parameters were also needed to begin the iteration procedure. Taking the limit of equation (33) as f/σ approaches zero and infinity respectively gives

$$\lim_{f/\sigma \to 0} Y_r/\sigma = A_3' \tag{34}$$

$$\lim_{f/\sigma \to \infty} Y_r/\sigma = A_2' + A_3' \tag{35}$$

which implies that A_2 and A_3 can be estimated from the asymptotes of Y_r/σ versus f/σ. Once this is done, it is simple to estimate A_1 by using a point on the graph that is not close to the asymptotes. Typical values of the fitted parameters are shown in Table 1, where D is the diameter of the coil.

The fitted curves are shown in figures 7, 8 and 9. The lower asymptote represents the contribution to Y_r due to eddy currents only since it is given by $A_3' = (\sigma R_e)^{-1}$. The upper asymptote represents the high frequency or low conductivity limiting case and again Y_r is simply proportional to σ. We believe that this method of presenting the data shows more clearly than earlier presentations (Gadian and Robinson, 1979; Vermeulen and Chute, 1983) the different asymptotic behaviour as f/σ approaches zero and infinity.

The agreement between the data and the fitted curves for the smaller coils (<3cm in diameter) shows that the

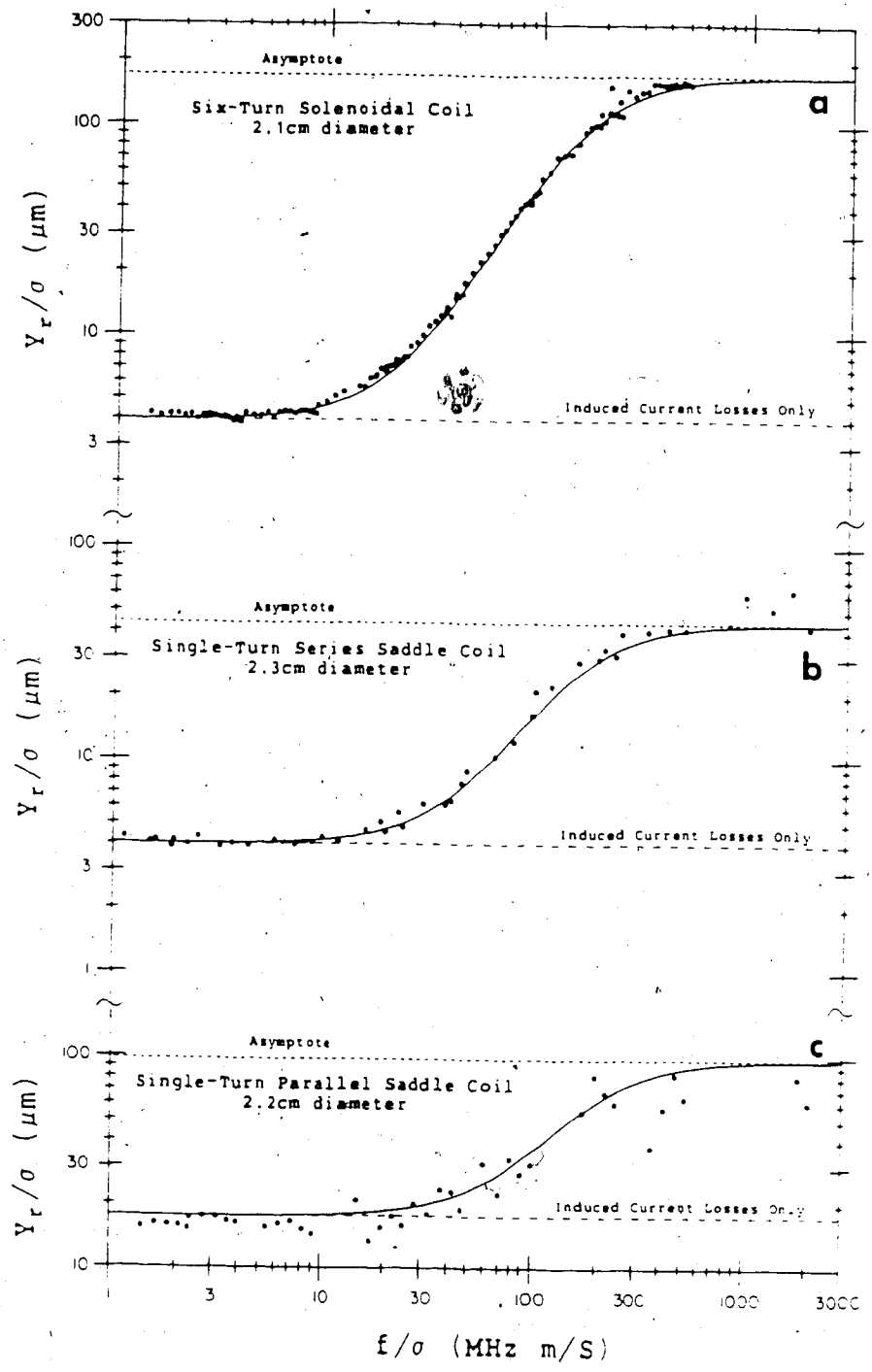

Figure 7. Plots of Y_r/σ versus f/σ for (a) the six-turn solenoidal coil (b) the 2.3cm diameter series saddle coil (c) the 2.2cm diameter parallel saddle coil. The solid curve shows the three parameter least squares fit.

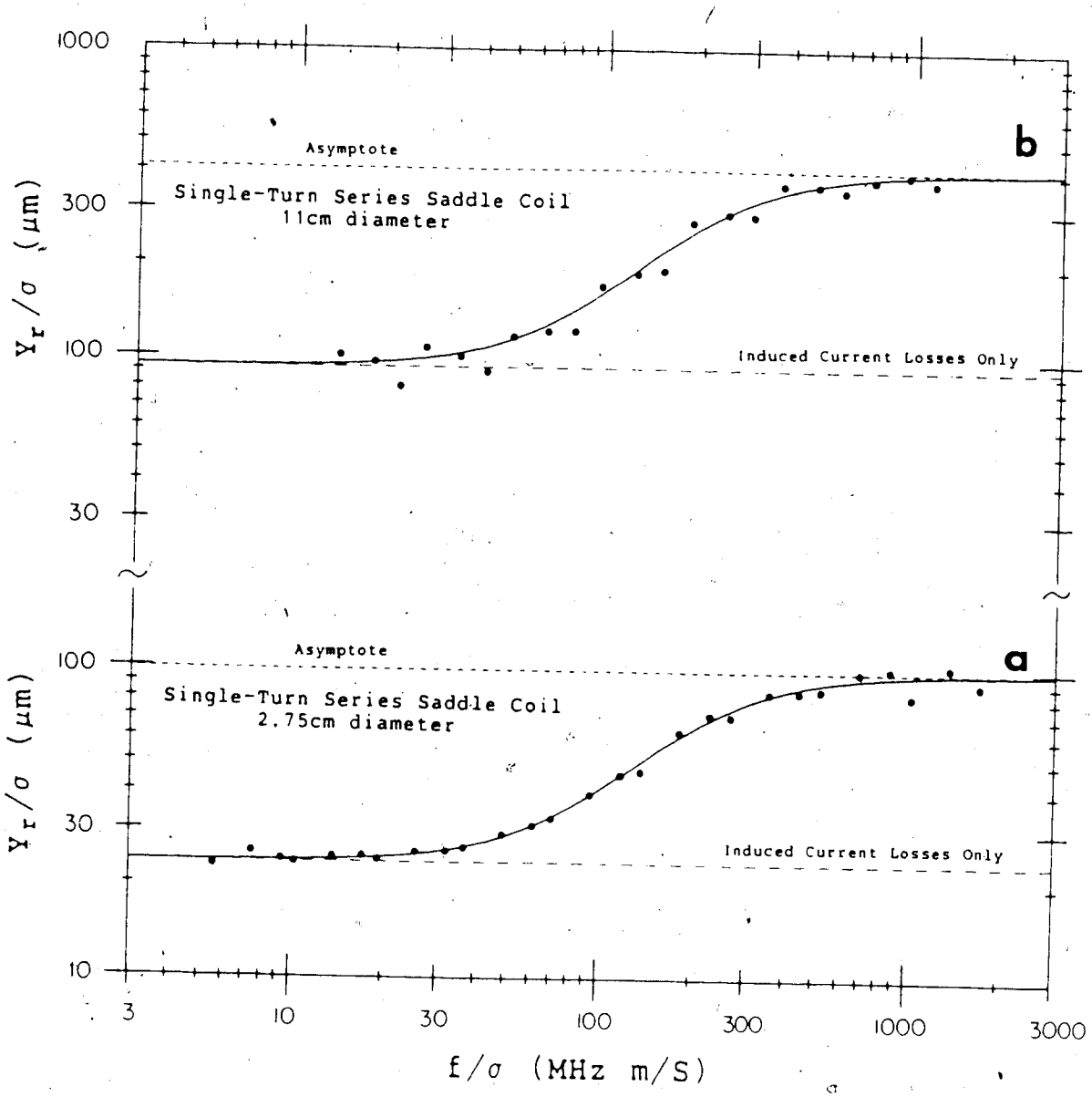

Figure 8. Plots of Y_r/σ versus f/σ for (a) the 2.75cm diameter series saddle coil (b) the 11cm diameter series saddle coil. The solid curve shows the three parameter least squares fit.

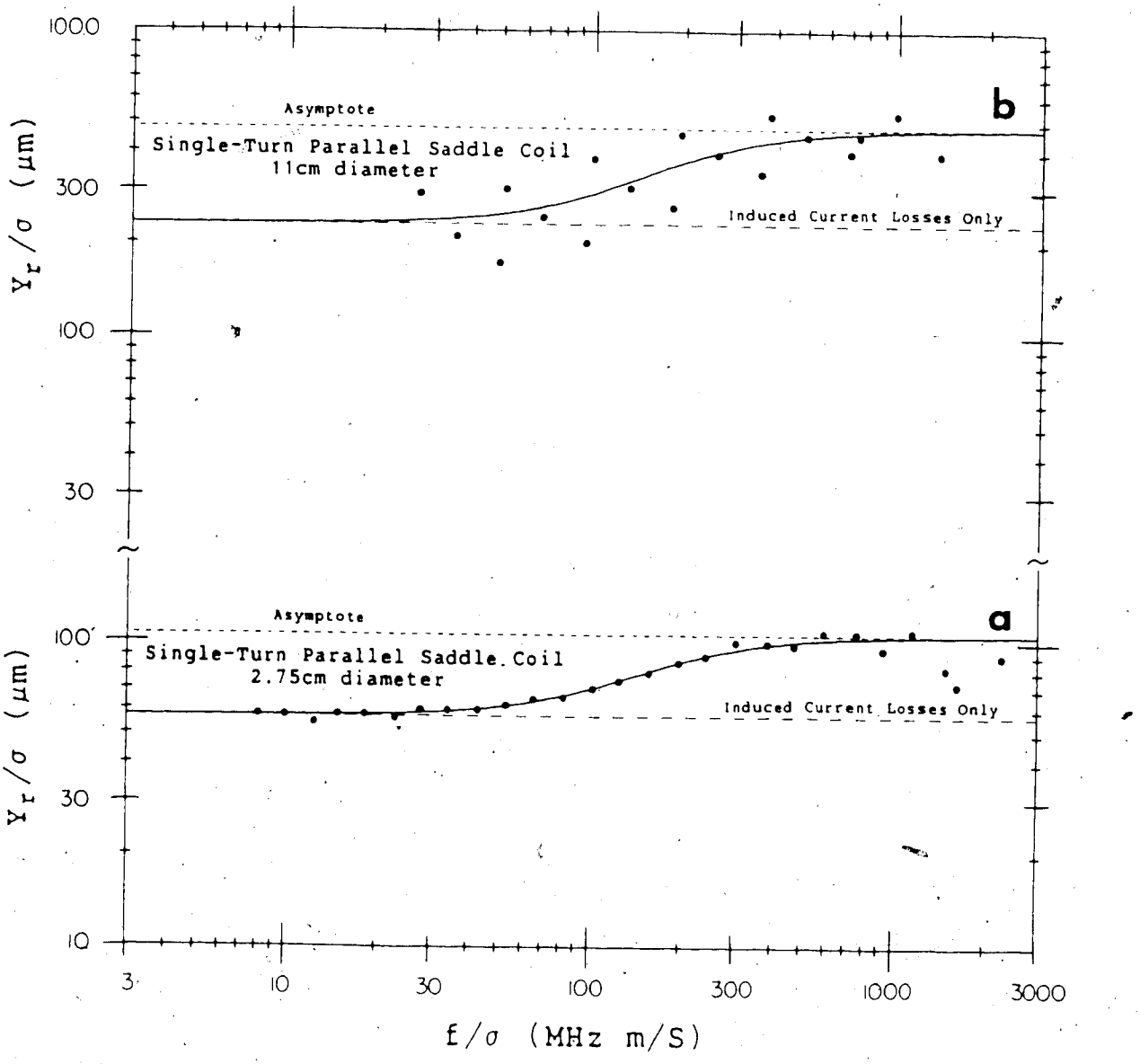

Figure 9. Plots of Y_r/σ versus f/σ for (a) the 2.75cm diameter parallel saddle coil (b) the 11cm diameter parallel saddle coil. The solid curve shows the three parameter least squares fit.

Table 1. Values of the fitted parameters.

Coil	D(cm)	L(μH)	$A_1(\Omega^2 Hz^2 m)$	$A_2(m^{-1})$	$A_3(m^{-1})$
six	2.1	0.762	1.41×10^{20}	5.96×10^{3}	2.52×10^{5}
ss	2.3	0.245	5.45×10^{20}	2.50×10^{4}	2.49×10^{5}
ps	2.2	0.0675	4.16×10^{20}	1.25×10^{4}	5.69×10^{5}
ss	2.75	0.267	4.48×10^{20}	1.32×10^{4}	4.22×10^{4}
ps	2.75	0.0800	5.59×10^{20}	2.06×10^{4}	1.75×10^{4}
ss	11.0	0.496	1.05×10^{20}	3.15×10^{3}	1.07×10^{4}
ps	11.0	0.304	1.23×10^{20}	4.04×10^{3}	4.30×10^{3}

six = six-turn solenoid

ss = series saddle coil

ps = parallel saddle coil

assumed circuit model is a good approximation for these coils. However, the data points for the larger coils appear to be arranged in triplets, each one corresponding to three frequencies and one sample conductivity. We believe that this is due to skin depth effects which were ignored in the model. At higher frequencies, the electromagnetic radiation of the coil will not penetrate as far into the sample and the losses will be smaller. This agrees with the decreasing trend seen for each triplet. A calculation of the skin depth $\delta_s \cong \sqrt{(2/\mu_o \omega \sigma)}$ at 50 MHz for a conductivity of 1.0 S/m gives a skin depth of approximately 7.1cm which, since it is comparable to the dimensions of the large coils and samples, implies that skin depth effects are probably the reason for the deviation from the predictions of the simple model.

B. Calculation of the heating caused by rf pulses

Graphs of the estimated temperature rise per pulse calculated using equation (22) are shown in figures 10, 11 and 12 for the various coil configurations analyzed in the previous section. The broken curves represent the contribution of eddy currents only and the solid curves represent the total heating. The contribution of the eddy currents is shown because it is possible, by inserting a Faraday shield between the coil and the sample, to effectively short circuit the secondary electric field of the coil (Pandey and Hughes, 1984), leaving only the eddy current contribution. The graphs were plotted assuming a

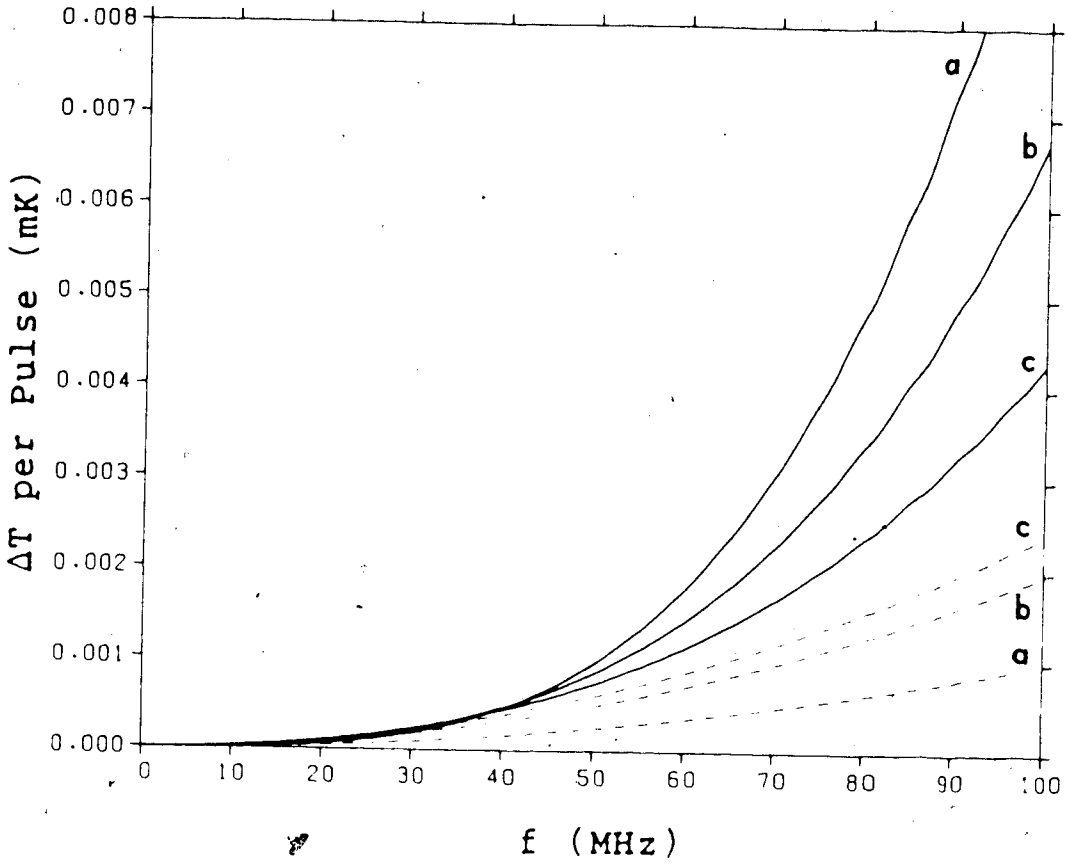

Figure 10. Calculated frequency dependence of the temperature rise for a sample with σ=1.2 S/m subjected to a 20μs $\pi/2$ pulse for protons in (a) the six-turn solenoidal coil (b) the 2.3cm diameter series saddle coil (c) the 2.2cm diameter parallel saddle coil. The broken curves represent the contribution to the heating due to induced currents only.

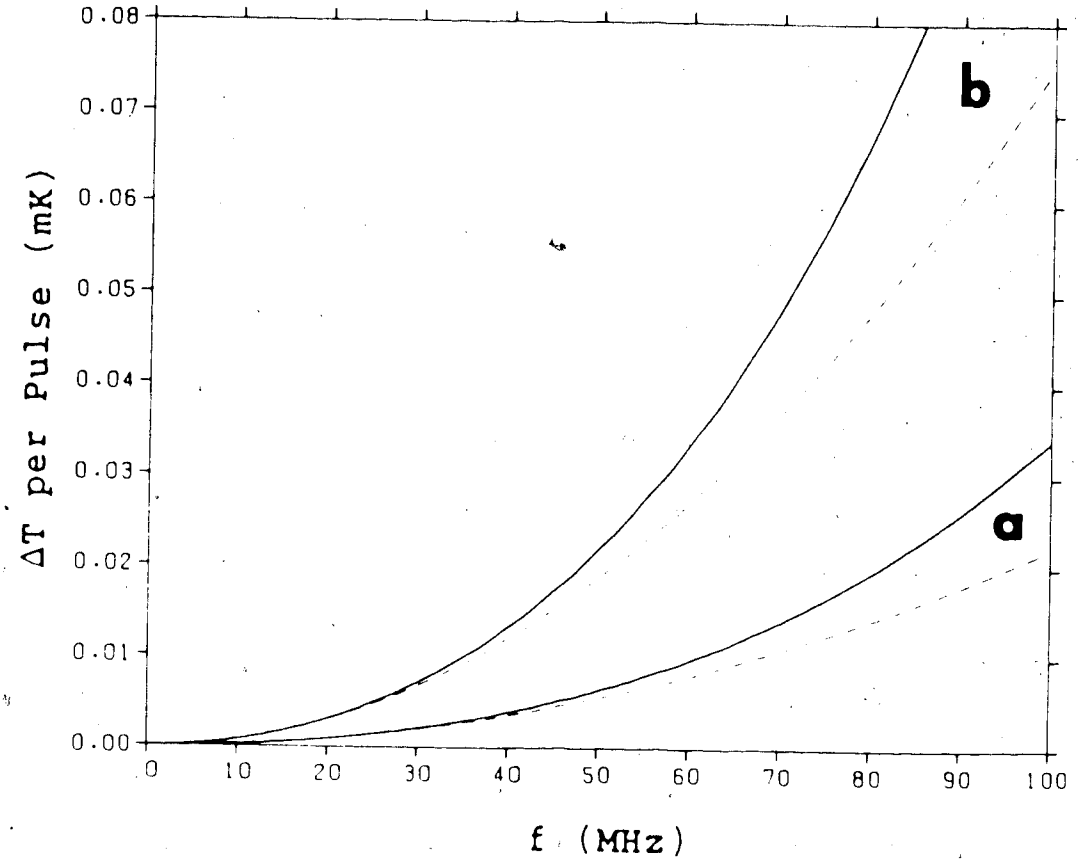

Figure 11. Calculated frequency dependence of the temperature rise for a sample with σ=1.2 S/m subjected to a 20μs $\pi/2$ pulse for protons in (a) the 2.75cm diameter series saddle coil (b) the 11cm diameter series saddle coil. The broken curves represent the contribution to the heating due to induced currents only.

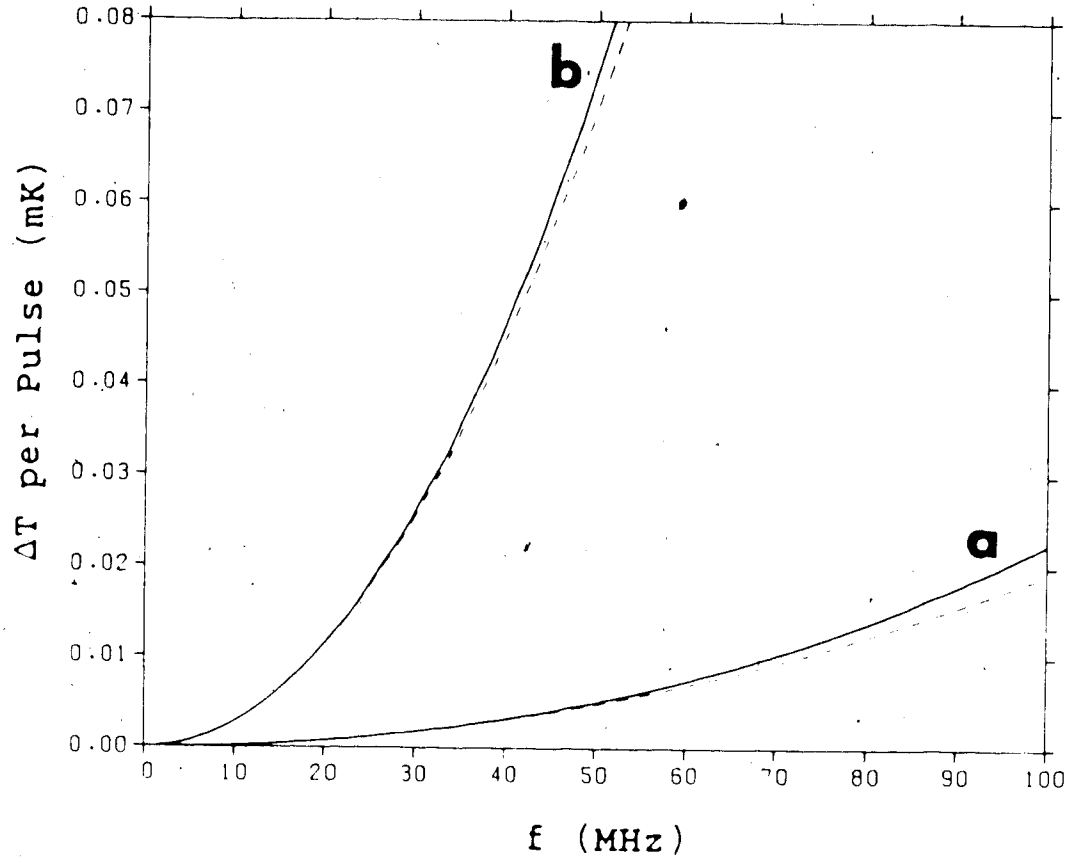

Figure 12. Calculated frequency dependence of the temperature rise for a sample with σ=1.2 S/m subjected to a 20μs $\pi/2$ pulse for protons in (a) the 2.75cm diameter parallel saddle coil. (b) the 11cm diameter parallel saddle coil. The broken curves represent the contribution to the heating due to induced currents only.

conductivity of 1.2 S/m, a typical value for biological tissue (Gadian and Robinson, 1979), and a $\pi/2$ pulse length of 20μs for protons. The field per unit current was calculated using a current sheet approximation for the solenoidal coil. The formula given by Mansfield and Morris (1982) was used to calculate the field per unit current for the saddle coils. The thermal capacity of the sample was assumed to be that of water. The inductance was calculated using a linear least squares fit (Squires, 1968) of C versus f^{-2}, and Y_r was calculated from equation (15) using the parameters in Table 1.

The first thing that can be noticed in figure 10 is the approximately two to one ratio of the eddy current heating due to the saddle and six turn coils, for the same sample. This is in agreement with the calculations in chapter II for the cylinder parallel and perpendicular to the magnetic field. The eddy current heating due to the series and parallel saddle coils are expected to be identical, but the parallel case exhibits $\simeq$20% greater heating. As can be seen in figure 7, the scatter in the data for the parallel saddle coil is quite large. For this reason, we believe that this difference is due to experimental error. This is confirmed by figures 11 and 12, where it can be seen that the small series saddle coil has slightly higher heating than the small parallel coil.

Using equation (3) of Vermeulen and Chute (1983) and our equation (22), it can be shown that if the number of

turns of a long solenoid is increased, keeping the dimensions of the solenoid constant, the eddy current heating will remain the same but the heating due to the secondary electric field will increase. This; and the fact that the coil-sample gap is smaller for the six turn coil, could explain the much larger total losses for the six turn solenoid. Evidently, it is particularly important that Faraday shields be used in *in vivo* NMR experiments using solenoidal coils. The smaller total losses of the parallel saddle coil compared to the series saddle coil is due to the parallel configuration which allows less charge buildup on the coil and decreases the secondary electric field through the sample (Redpath and Hutchison, 1984). This shows that a parallel configuration is preferred as far as heating is concerned if no Faraday shield is used.

C. Size dependence of the heating caused by rf pulses

It is possible to estimate the heating to be expected in larger coils of similar geometry to ours using the fact that the heating should scale as λ^2 (see §II.E). By scaling the results shown in figure 10, it can be shown that for a 23cm series saddle coil with 100 MHz 20μs $\pi/2$ pulses applied every 20ms, the heating would be 0.8°C/min for a sample of diameter 16cm and length 53cm (Antolak, Hughes and Allen, 1985). This would certainly be cause for alarm since a typical *in vivo* NMR experiment would last about 20 minutes. In fact, regions near the surface of the sample are expected

to absorb more energy than the interior of the sample, (see §II.C), so the problem may be more serious there. If the heat conductivity of the sample is not very large, then these areas will heat up more quickly than the interior regions.

The size dependence of the calculated heating caused by radio frequency pulses was tested using saddle coils of diameter 2.75cm and 11cm. The heating is expected to increase as λ^2 which is 16 for this experiment. In the parallel case, the heating due to the large coil is about 14.4 times as large as for the small parallel saddle coil, and this is quite close to the expected value. However, the heating in the larger series saddle coil is only about 3.5 times as large as for the small coil. In equation (22), the only measured quantities are L and Y_r. It can be seen in figures 8 and 9 that Y_r is proportional to λ as expected. The inductance L is expected to scale as λ also, but the ratios of the inductances, as shown in Table 1, are $\simeq$1.86 and $\simeq$3.8 for the series and parallel configurations respectively. Squaring these numbers gives 3.5 and 14.4 respectively, which correspond to the ratios of the calculated heating per pulse. The 11cm diameter series saddle coil was subsequently rewound and its inductance found to be 1.02μH as opposed to the previously measured value of 0.496μH. The reason for the discrepancy is not known. Possibly, the wires leading from one loop to the other on the 11cm diameter series saddle coil, as previously

wound, were too close together at the crossover point resulting in a capacitance between the wires which tended to short-circuit one loop of the coil. The latest measured value of 1.02μH, is about 3.8 times the inductance of the smaller series saddle coil and is much closer to the expected value. Because of the error found in the previously measured inductance, Y_r was remeasured for two of the samples. However, these values were found to agree with the data shown in figure 8, within experimental error. If we therefore assume that the above values of the parameters A_1, A_2 and A_3 are still valid, then the heating in the larger series saddle coil should be $3.5x(1.02/0.496)^2$ or 14.8 times as large as for the smaller series saddle coil. This is much closer to the expected value.

D. Comparison of the heating produced by two variants of a commonly used imaging technique

A commonly used *in vivo* NMR imaging technique uses a long so-called selective $\pi/2$ pulse (also called a soft pulse) in the presence of a linear magnetic field gradient to select a slice which is to be imaged (Mansfield and Morris, 1982). The signal is refocussed to produce an "echo" in either of two ways, by applying a π pulse, or by reversing the magnetic field gradient. However, the π pulse must be short (a so-called hard pulse) to ensure that the defocussing effect of the field gradient during the pulse is negligible. Typical pulse lengths are 1ms for the soft $\pi/2$

pulse and 40μs for the hard π pulse (Allen, 1985). Since the heating per pulse is inversely proportional to the pulse length, it follows that the temperature rise using a hard π pulse for refocussing is roughly one hundred times larger than that caused if refocussing is achieved by reversing the field gradient. Thus, the switched field gradient method is far superior to the π pulse method, as far as rf heating is concerned.

Chapter V

Conclusion

It has been shown that the radio frequency energy deposition in saline phantoms can be modelled successfully for small coils using a very simple lumped circuit model with only three parameters. As the coil size is increased to dimensions comparable to those used in *in vivo* NMR studies, deviations from the model are observed which are attributed to skin depth effects. By scaling our data, it has also been shown that radio frequency heating *is* a possible danger in *in vivo* NMR for frequencies approaching 100MHz.

The next logical step in this investigation is to refine the model giving some frequency dependence to A_1, A_2 and A_3. Other modifications may also be needed where the wavelength of the radiation becomes comparable with the sample dimensions. More theoretical and experimental work is needed to gain a greater understanding of this heating phenomenon.

References

Allen, P.S., 1985, private communication.

Antolak, J., Hughes, D.G., and P.S. Allen, 1985, **Proceedings of the International Conference on Magnetic Resonance in Cancer (April 30 - May 4, 1985, Banff, Alberta)**, (in press, Pergamon, New York).

Bevington, P.R., 1969, **Data Reduction and Error Analysis for the Physical Sciences** (McGraw-Hill: New York).

Bottomley, P.A., Redington, R.W., Edelstein, W.A., and J.F. Schenk, 1985, **Magnetic Resonance in Medicine** 2, 336.

Chambers, J.F., Stokes, J.M., and R.H. Stokes, 1956, **Journal of Physical Chemistry**, 60, 985.

Chute, F.S., and F.E Vermeulen, 1981, **IEEE Transactions on Education**, E-24, 278.

Chute, F.S., Vermeulen, F.E., and M.R. Cervenan, 1981, **Canadian Electrical Engineering Journal**, 6, 20.

Coupland, R.E. et al., 1983, **The British Journal of Radiology**, 56, 974.

Gadian, D.G., and F.N.H. Robinson, 1979, **Journal of Magnetic Resonance**, 34, 449.

Gandhi, O.P., 1975, **IEEE Transactions on Biomedical Engineering**, 22, 536.

Ginsberg, D.M., and M.J. Melchner, 1970, **The Review of Scientific Instruments**, 41, 122.

Mansfield, P., and P.G. Morris, 1982, **NMR Imaging in Biomedicine** (Academic Press: New York).

Pandey, L., and D.G. Hughes, 1984, **Journal of Magnetic Resonance**, 56, 443.

Redpath, T.W., and J.M.S. Hutchison, 1984, **Magnetic Resonance Imaging**, 2, 295.

Reitz, J.R., Milford, F.J., and R.W. Christy, 1979, **Foundations of Electromagnetic Theory** (Addison-Wesley: Reading, Massachusetts).

Robinson, R.A., and R.H. Stokes, 1959, **Electrolyte Solutions** (Academic Press: New York).

Schwan, H.P., 1982, **Journal of Microwave Power**, 17, 1.

Squires, G.L., 1968, **Practical Physics** (McGraw-Hill: London).

Vermeulen, F.E., and F.S. Chute, 1983, **Canadian Electrical Engineering Journal**, 8, 93.